Numerical and Experimental Investigation of Large Stratified Thermal Storage Systems in transient states

Robin Fick[1,*], Robert Honke[1], Dieter Brüggemann[2]

[1] *University of Applied Sciences Hof, Institute for Hydrogen and Energy Technology, Hof, Germany*
[2] *University of Bayreuth, Center of Energy Technology, Bayreuth, Germany*
[*] *Corresponding author. Email: robin.fick.2@hof-university.de*

ABSTRACT

Mid-sized thermal energy storage (TES) systems, especially in the distributed sector, have received little attention for public buildings. Validation of such systems, especially for the use of multiple renewables with different operating modes using CFD simulations, is still pending. The objective of this study is to validate a CFD model for the operation of complex and mid-sized TES systems for simultaneous charging and discharging cycles to enable investigations on optimized operating modes, geometric optimizations, and predictive charging and discharging scenarios. For this purpose, the 60 m³ local heating storage of Großbardorf, Germany, was used to obtain real-time operating conditions and in-situ temperature distribution data. Charging and discharging cycles as well as combined scenarios were calculated and compared with the experimentally determined dynamics of the thermocline. Simulations were performed using the open-source tool OpenFOAM® with the single-phase transient solver buoyantPimpleFoam in laminar and turbulent modes, including ambient heat losses. Good agreement was found between simulated and experimental data, especially in the regions of layer transitions with a RMSE of 1.2 °C or less over the entire observation period. It is shown how the validation allows further improvements and optimizations of TES with greater confidence. In particular, for research on the efficient use of multiple, fluctuating renewable energies and the increase of self-sufficiency in the decentralized sector, a demand-optimized charging and discharging layout is presented for a mid-sized TES to be installed at the new Institute for Hydrogen and Energy Technology (iwe) at Hof University of Applied Sciences. By conducting research in facilities such as the iwe, this approach will not only create opportunities for the future deployment of renewable energy storage and related systems, but also highlight the importance of decarbonization in the decentralized sector.

Keywords: *Stratified Thermal Energy Storage, Computational Fluid Dynamics, OpenFOAM, Decentralized Sector, Optimized Use of Renewable Energies.*

1. INTRODUCTION

There has been significant progress in stratified thermal energy storage (TES) systems in recent years, but rather only for very small storage units, e.g., for single- and multi-family dwellings [1, 2, 3, 4], or for large seasonal storage units [5, 6, 7, 8]. However, there is a significant lack of validated computational fluid dynamic (CFD) models, besides a few one-dimensional models [9, 10], to study and optimize the thermocline behavior of medium-sized stratified TESs, especially those with capacities larger than 50 m³, like those e.g., used in public buildings. To address this gap, this work validates a CFD model to properly simulate volatile charging, discharging, and simultaneous events in larger stratified TESs. Validation of such a model is essential for the development of more efficient and complex models for predicting storage states. By improving the efficiency and performance of stratified TES, the potential of the study should help reduce energy consumption in larger public buildings, contributing to the decarbonization of the building sector. These systems, with significant energy demands, offer a valuable opportunity for efficiency improvements through the integration and optimization of stratified TES [3, 11, 12].

Techniques such as stratification lances, radial diffusers, and other advanced approaches have been explored to improve the performance of stratified thermal energy storage systems. Extensive research has been conducted to understand the underlying principles

P. Droege and L. Quint (eds.), *Proceedings of the International Renewable Energy Storage and Systems Conference (IRES 2023)*, Atlantis Highlights in Engineering 32,
https://doi.org/10.2991/978-94-6463-455-6_13

and optimize these systems [5, 12, 13, 14, 15, 16]. However, there is still a gap in knowledge, particularly with respect to the internal effects and behavior of medium-scale stratified heat storage systems.

The use of CFD for numerical modeling is proving beneficial in studying the intricacies and challenges associated with stratified thermal storage [1, 2, 3, 8, 17, 18]. Consequently, CFD enables comprehensive investigations of many parameters and improves the design of charging systems and operating scenarios prior to construction. This approach proves superior in situations characterized by multiple heat sources, complicated charging configurations, and transient operating conditions. Even under challenging conditions, CFD models can provide valuable insight beyond the limits of direct observations.

Previous studies have investigated various aspects of this approach, including CFD model development, numerical methods, and validation experiments. Commercial software packages such as Ansys-CFX [19], COMSOL multiphysics, CFD-Fluent, and SolidWorks have been widely used in these studies, see Table 1 in [3]. These tools utilize the basic conservation equations of fluid mechanics and CFD, including the Navier-Stokes equations with consideration of buoyancy effects. The open-source platform OpenFOAM® also uses dedicated solvers for buoyancy effects such as "buoyantPimpleFoam" or "buoyantBoussinesque-PimpleFoam" for this purpose [8, 17, 20, 21].

However, many sources use only a limited set of boundary conditions for three-dimensional simulations and their validation. Typically, simulations are based on simplified, homogeneous internal temperature profiles [1, 2, 17] and steady-state inflow or outflow conditions that include temperature and volume flow rates to study only the pure charging or discharging behavior of TES. Nevertheless, most studies consider external heat losses [1, 3, 22], which cause convective flow effects near the storage walls.

In addition, [3] provides an overview of some two- or one-dimensional models developed to efficiently calculate internal temperature stratification, but again only for small and packed bed storages. Further one- or two-dimensional models can be found in [2, 9, 10, 11, 23].

Several parameters have been used to validate CFD simulations, including the temporal behavior of the thermocline with respect to the reservoir height [1, 3, 5, 10, 19]. The Richardson number (*Ri*) is a subtler parameter that is critical to the stability of the thermocline. Maintaining an *Ri* value greater than 1 indicates a stable thermocline [3, 12], and in [11] a *Ri* value greater than 5 is also supported by experimental correlation. Moreover, the validation parameters in [2, 19], which also deal with turbulence effects, focus on the Reynolds number (*Re*) for turbulence intensity mainly at the inlet and outlet ports.

Turbulence modeling in stratified heat reservoirs has also been studied in detail, focusing on buoyancy effects and challenges posed by different turbulence models. The main goal is to improve CFD predictions by accurately capturing the fluid dynamics in these reservoirs. The classical k-epsilon turbulence model has gained importance, especially when adapted to account for buoyancy effects. This model has shown good validation results in several studies [2, 5, 13, 24, 25], including models focusing, for example, on internal discharge coils [26]. However, the selection and parameterization of turbulence models, especially in conjunction with buoyancy effects, is critical. Numerical effects can lead to pronounced diffusion, which can bias the results [27]. However, the "buoyantKEpsilon" turbulence model within the OpenFOAM® version 8, which is optimized for these effects, provides a remedy for these challenges. This model can correct for biases or can be further customized with additional parameters for a more realistic representation.

CFD models of smaller buffer and stratified heat storage systems have been extensively studied, especially for applications in residential buildings such as single-family houses [1, 2, 3, 5]. This research has demonstrated the thermal performance and efficiency of the storage systems. Several studies have also shed light on the effective operation of small thermal storage systems and the design of charging devices [5, 14, 15, 28].

In addition, large-scale seasonal storage systems for district heating and cooling networks have also been studied to improve system performance and optimization [5, 6, 8]. However, research on large-scale thermal storage systems such as the known examples of TU Dresden and TU Chemnitz [29, 30] have additionally focused on the specifics of the system charging mechanism. Nevertheless, despite or possibly because of their simple charging methods, these larger storages have shown good agreement between modeling and experimental data, indicating their usefulness in their size range. However, the research gap is still large for medium scale stratified thermal storage systems. Few research papers have directly addressed simulation models for these storage systems. [14] did refer to a 50 m³ reservoir, but only in the context of additional CFD simulations and without direct experimental validation of the medium-sized storage. The existing literature emphasizes the need for further research on medium-sized heat storage systems, typically over 50 m³, as they appear in public buildings and similar applications [22, 31] also in combination with complex operating scenarios. Therefore, this study focuses on the particular problems and prospects of this size range of

stratified TES to overcome this gap. We develop and validate a 3D CFD model for this type of stratified heat storage. Despite the challenges in defining storage sizes, we will rely on validated models from different scales and turbulence models to adapt and validate them for our context.

The outline of the paper is as follows. Section 2 provides a detailed explanation of the CFD and experimental model and the validation process. Section 3 provides a detailed comparison between the simulation results and the experimental data and discusses the challenges and limitations encountered. Section 4 introduces the reader to the complex storage system of the new Institute for Hydrogen and Energy Technology at Hof University of Applied Sciences and shows how the results can contribute to a better understanding and implementation of such systems in the building sector. Finally, the last section summarizes the main results and their implications.

2. METHODS

The experimental part of this study was conducted using a 60 m³ heat storage tank for a local heating network (LHN) - a storage system that allows accurate evaluation of the thermocline formation and behavior. The selected CFD model and numerical methods are based on well-established and commonly used methods for simulating heat storages [8, 17, 20, 21]. The experimental and theoretical details are given below along with the description of the evaluation procedure.

2.1. Experimental set-up

For the experimental studies, a medium-sized sensible stratified TES in Großbardorf, Germany, was available as the central component of an LHN. The general layering of the TES consists of two inner sections leading to one thermocline. The reservoir has a diameter of 2.9 m and a total height of 9.6 m. It is insulated with 20 cm thick mineral wool and protected by 1 mm thick aluminum cladding. It is primarily fed by a combined heat and power (CHP) unit, which introduces hot water through a DN125 steel pipe bent upwards. The flow to the CHP unit is taken through an identical pipe at the bottom of the storage tank. The upper part is additionally equipped with a perforated pipe diffuser for heat extraction and a DN150 steel pipe, also bent downwards, for water recirculation at the bottom of the storage tank. The assumed thermophysical properties of the materials used are listed in Table 1. During dynamic operation, an ensemble of six strategically positioned temperature sensors within the storage system recorded temperature profiles at one-minute intervals. (see Figure 1)

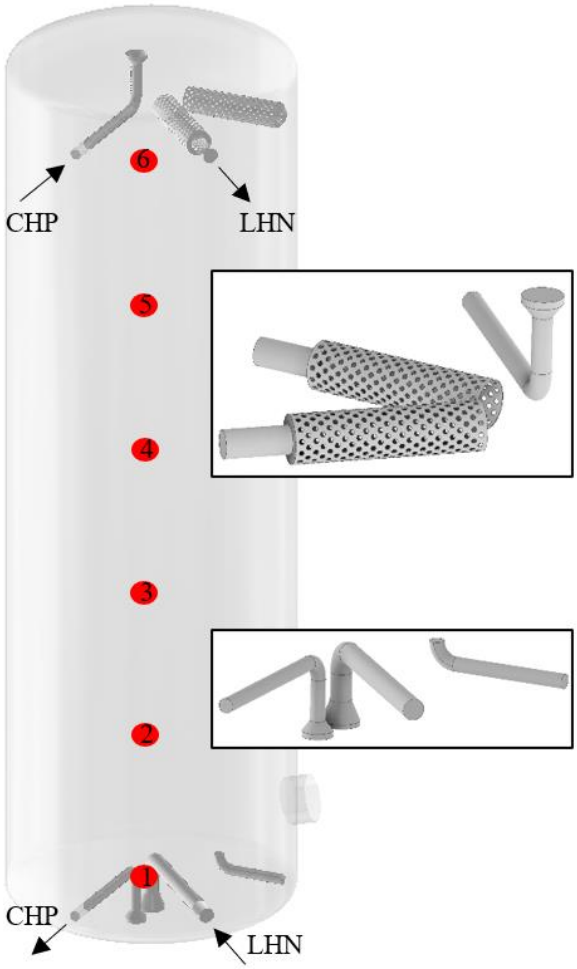

Figure 1 Storage geometry without insulation incl. sensor positions.

Table 1. Material properties of storage wall layout

Material	Therm. conductivity (W/m/K)	Thickness (m)
steel	45	0.018
insulation	0.035	0.2
alu. casing	160	0.001

The LHN is operated in 2 modes. In winter mode, it is continuously supplied with heat, while in summer, heat is only supplied to individual houses at certain times. The study examined different scenarios derived from the standard operation of the storage tank, winter mode, without artificially induced scenarios. Accordingly, the data for validation and analysis were based on actual operating conditions. The validation experiment included three operating cases: (1) charging the TES alone ("charging"), (2) discharging only ("discharging"), and (3) a configuration that included both charging and discharging the storage tank ("simultaneous"). Careful compilation of the experimental scenarios within specific

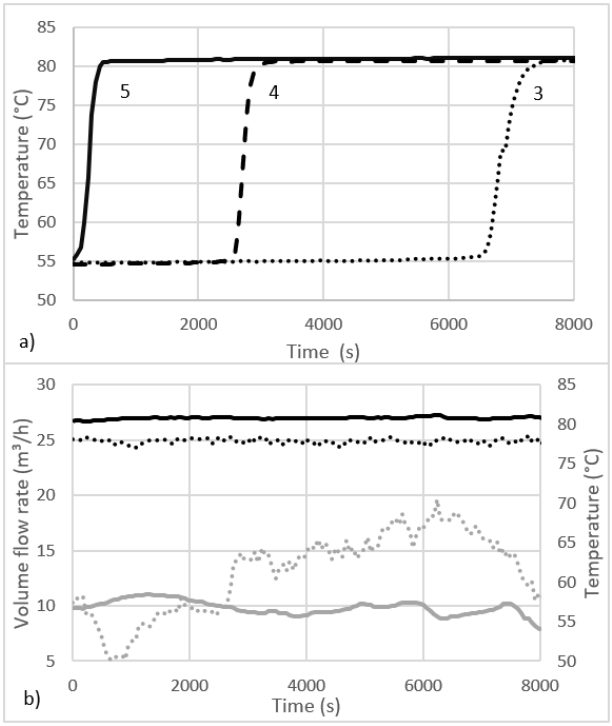

Figure 2 Simultaneous scenario: a) transient temperature at sensors 5, 4 and 3 over observation time starting at June 3rd, 2023, 07:01 pm; b) volume flow rate (dotted) and temperature profile (solid) of CHP (black) and LHS (grey).

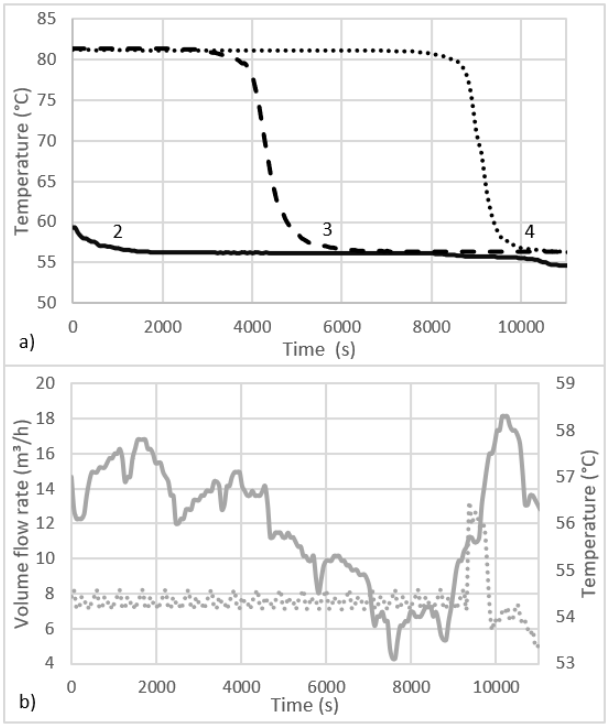

Figure 3 Discharging scenario: a) transient temperature at sensors 2, 3 and 4 over observation time starting at June 2nd, 2023, 11:38 am; b) volume flow rate (dotted) and temperature profile (solid) of LHN feeding the TES.

time frames provided a comprehensive data set that was critical for rigorous validation of the computational simulations.

The measurement and control system ("Neuberger") used standard PT100 sensors to monitor temperature profiles at the six storage locations shown in Figure 1. Thermal interactions with the CHP unit were captured using an Elster F96 Plus US heat meter. An ultrasonic flow meter (Katronic KATflow 230) was used to measure forward flow into the district heating network with a documented maximum measurement tolerance of 3%. Minute-interval data enabled the identification of centimeter-scale temperature transitions, which were used as initial conditions for the computational model's thermal stratification and validation process. The experimental campaign spanned from the 2nd to the 4th of June in 2023 (still in winter mode), encapsulating a meticulous sequence of operational periods.

Considering the operating context of the district heating network during the winter period, an almost continuous heat extraction for the district heating network prevailed. This dynamic operating scenario provided a suitable framework for investigating the system behavior in different operating modes, which included both discharging and simultaneous scenarios. Figure 2 and Figure 3 highlight these two scenarios.

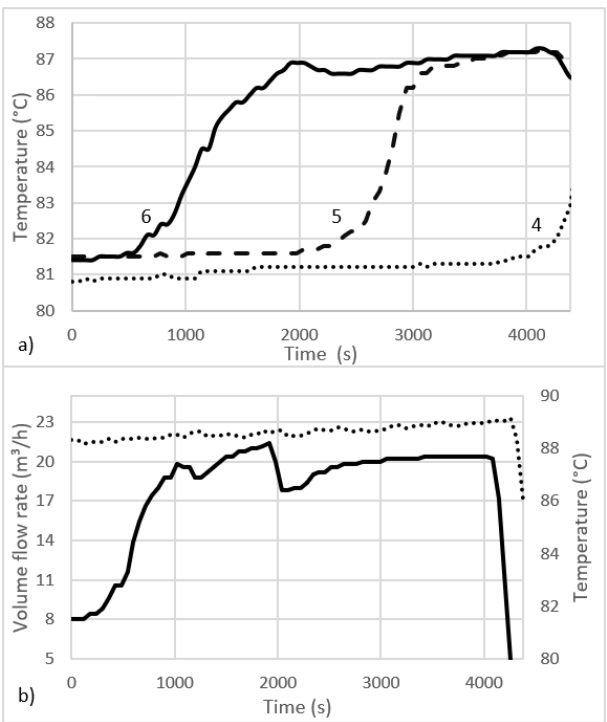

Figure 4 Charging scenario: a) transient temperature at sensors 6, 5 and 4 over observation time starting at June 3rd, 2023, 10:53 pm; b) volume flow rate (dotted) and temperature profile (solid) of CHP.

However, the selection of an exclusive charging cycle posed a certain difficulty in the operation mode considered. Therefore, a specific interval was identified during which the storage system was already heavily charged and reached an overall largely homogeneous temperature of about 81.5 °C in the upper section. During this period, the heat supply from the CHP plant continued, resulting in a slightly elevated inlet temperature of over 86 °C. Accordingly, a further, new thermocline formed during the charging process, which moved continuously downward in the storage tank during the observation period. (see Figure 4)

2.2. CFD-Model set-up

The reservoir was reconstructed in a common CAD program based on original design drawings. The individual areas or patches were then extracted, defined as stereolithography (stl) files, and further processed using OpenFOAM®'s in-house meshing algorithm, "SnappyHexMesh", which produces a homogeneous, hexahedral-dominated mesh. The domain had about 700000 cells with an initial element edge length of about 4.8 cm.

In order to capture the flow features of interest with adequate resolution, the inlet and outlet regions as well as the internal charging and discharging geometries were refined by a factor of 2. This refinement was intended to achieve an accurate representation of the internal flow profiles, including near-wall representations. In addition, adaptive mesh refinement was applied to perform refinement based on an internally calculated temperature gradient, which is naturally highest in the thermocline region. Excessive numerical drift or diffusion effects were thus eliminated by providing sufficient grid resolution along the elevation axis of the reservoir. In a separate mesh study, the quality of the results with this meshing approach is well related to the numerical computational effort. Here, the doubly refined hexahedral mesh size in the region of the thermocline, inflows and outflows corresponds to about 1.2 cm and ends with a total of only about 800000 elements (see Figure 5).

As for the initial and boundary conditions for the temperatures, the initial temperature stratification within the reservoir was set for the entire computational domain using the "setFields" tool in OpenFOAM®. To ensure sufficient accuracy, the results for the location of the thermocline were exactly aligned with the real measurement times. Boundary conditions such as inlet and outlet temperatures and volume flow rates were adjusted to the actual varying charging and discharging profiles. The inlet temperatures into the TES are based on experimentally determined real values, where these were linearly interpolated for instantaneous simulation time steps. Since the entire storage tank was filled without any additional air inside, the heat loss of the

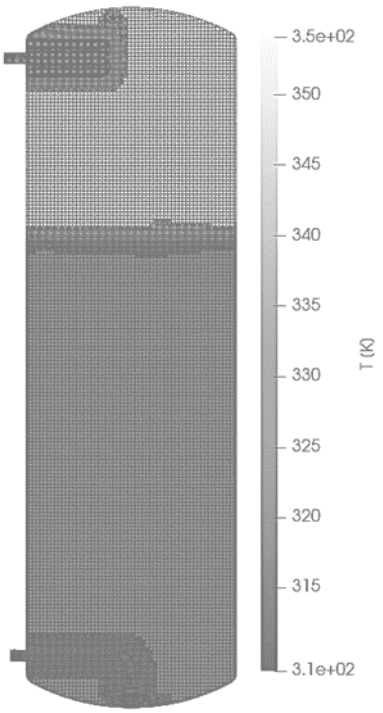

Figure 5 Mesh incl. adaptive mesh refinement of thermocline of simultaneous scenario after 1450 s at 6.4 m; above thermocline: T > 80 °C, below thermocline: T < 56 °C.

entire storage wall (bottom, top and circumferential sides) was modeled with the boundary condition “externalWallHeatFluxTemperature". The heat loss calculation takes into account the different material properties (steel, mineral wool insulation, aluminum cladding), their respective thicknesses, and the averaged ambient temperature leading to external heat losses. All additional internal geometries that are not relevant for the current loading condition were defined as gradient-free and contribute only insignificantly to the temperature fluctuations.

Similar to the temperature boundary conditions, the velocities for the charging and discharging fluids were given on the basis of experimentally derived and linearly interpolated data. Preliminary tests showed that a realistic internal flow profile was established after a period of 10 minutes, which formed the basis for subsequent analyses. These case individual pre-simulations were adjusted such that the transition of the thermocline specifically occurred at the desired time for a given temperature sensor (see Figure 6). A "noSlip" boundary condition was applied to the outer wall and to all internal charging, discharging, or perturbation geometries to account for zero velocity at the wall.

Prior to the actual evaluation simulation, an internal pressure field was imposed on the entire domain. During the initial transient phase (within the first simulated seconds), this pressure field adjusted to a height-

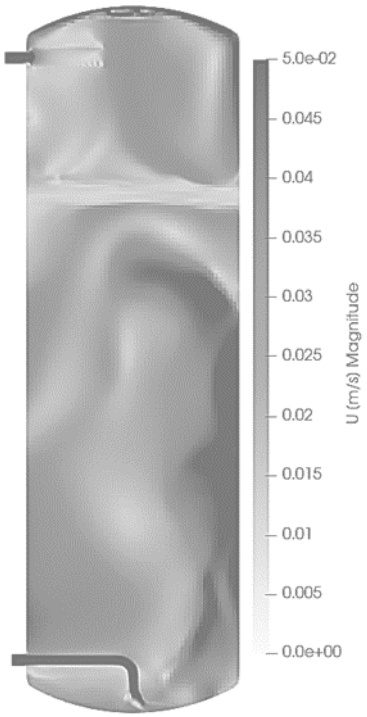

Figure 6 Velocity profile after initialization simulation of 600 s of simultaneous scenario.

dependent pressure gradient over the entire height of the reservoir due to hydrostatic effects. This initialization process provided a realistic pressure distribution within the domain before the start of the main simulation.

The computational framework used for the flow simulations relies on the capabilities of OpenFOAM® version 8 and uses the transient single-phase solver "buoyantPimpleFoam" [32]. This solver is able to account for compressible media along with turbulence and heat transport phenomena both within the computational domain and across its boundaries. It is based on the finite volume method and seamlessly integrates buoyancy and heat conduction effects.

At its core, the solver essentially comprises the well-known Reynolds-averaged Navier-Stokes equations for three-dimensional fluid dynamics, which take into account the principles of conservation of mass, momentum and energy [33]. However, to account for the details of turbulence, the solver includes an additional two-equation turbulence model called "buoyantKEpsilon". This turbulence model is most notable for its fit to buoyancy-related effects that are primarily based on density gradients rather than temperature gradients. In this context, the model introduces another parameter, usually referred to as "Cg", which replaces the conventional "1/Pr" term, with the default value of "Cg" set to 1 in all studies [34]. Following [17], a turbulence intensity of 5% instead of 3% was assumed for the inlets, since higher velocities prevail in these scenarios.

Table 2. Discretization schemes of fvSchemes-dict

Formulation	**Scheme**
Time derivative schemes	Default Euler
Gradient schemes	Cell-limited Gauss linear, coefficient = 1
Schemes for divergence of U, h, e, k, p, epsilon	Gauss linear Upwind limited
Schemes for divergence of the deviatoric stress tensor	Gauss linear
Laplacian schemes	Gauss linear corrected
Interpolation schemes	Linear
Surface normal gradient schemes	Corrected
Wall distances schemes	Mesh wave

Table 2 lists the particular discretization schemes used to solve the above conservation equations in OpenFOAM-specific formulation.

Pressure-based solvers found in the hydrostatic pressure category use the Preconditioned Conjugate Gradient (PCG) solver and the Diagonal-based Incomplete Cholesky (DIC) preconditioner. The convergence criteria are set by the tolerance and relative tolerance parameters as $1e^{-5}$ and $1e^{-2}$, respectively. The final hydrostatic pressure category inherits the previous settings but finalizes the pressure correction with the relative tolerance set to zero.

For momentum, turbulence, and scalar transport solvers, the Stabilized Preconditioned Bi-Conjugate Gradient (PBiCGStab) solver is used with the Diagonal-based Incomplete Lower and Upper part (DILU) preconditioner. The convergence criteria are set by the tolerance and relative tolerance with $1e^{-6}$ and $1e^{-2}$, respectively. Similarly, the final values adopt the settings of the non-final version, with the relative tolerance also set to zero.

Acceptable solution stability was achieved by introducing additional relaxation factors. Specifically, a relaxation factor of 0.3 was used for the iterative calculation of hydrostatic pressure, internal energy, turbulent kinetic energy, and velocity fields. The buoyantPimpleFoam solver was operated in PISO (pressure-implicit with splitting of operators) mode with two inner and one outer non-orthogonal correction loops.

2.3. Evaluation procedure

The following approaches were used to evaluate the validation results: (1) the transient evaluations of thermocline transitions at individual sensors and their quantitative evaluation using root mean square error (*RMSE*) to account for transient variations, (2) the Reynolds numbers of inlets and outlets, (3) the Reynolds number of the thermocline related to reservoir diameter, and (4) the Richardson number (*Ri*) to evaluate thermocline quality.

The time variation of the measured values from the temperature sensors allows to determine the position, and the velocity of the thermocline. The quality of the simulation results compared to the experimental data set throughout the observation period was evaluated by analyzing the *RMSE* of the temperature values over all discrete time steps. The *RMSE* is calculated according to Equation (1), where n is the number of measurements or time steps and E_i are the experimental and S_i are the simulated values of each measurement.

$$RMSE = \sqrt{\frac{1}{n}\sum_{1=1}^{n}|E_i - S_i|^2} \tag{1}$$

Reynolds numbers (*Re*) were calculated and compared to capture the flow dynamics and turbulence in the inlets of the CHP and LHN of the storage system. The *Re* results should help to extrapolate the results to other stratified thermal storage systems in the future, including those with much lower volumetric flows. *Re* is calculated by Equation (2), where v_{inlet} is the maximum flow velocity into the storage tank averaged over the pipe diameter, the pipe diameter d_{inlet} itself is the characteristic length and ν_W is the kinematic viscosity of water at corresponding inlet temperatures.

$$Re = \frac{v_{inlet} d_{inlet}}{\nu_W} \tag{2}$$

In addition to the high Reynolds numbers at the inlets and outlets, a measure was defined to evaluate the unsteady behavior of the thermocline. The thermocline Re_{th} is calculated by Equation (3), where $v_{z_{th}}$ is the diameter averaged vertical velocity of the thermocline, d_{st} is the inner storage diameter and ν_{W_a} is the kinematic viscosity at average temperature of the thermocline based on studies by [16] and [25].

$$Re_{th} = \frac{v_{z_{th}} d_{st}}{\nu_{W_a}} \tag{3}$$

The Richardson number (*Ri*) was calculated and analyzed using the method described in [3] to compare the quality of the thermocline with published values. *Ri* values above 1 indicate more stable thermocline behavior, where potential energies exceed kinetic energies [3, 12]. $Ri > 5$ is considered a stable thermocline value in [11]. *Ri* is calculated according to Equation (4), where β_f is the thermal expansion coefficient, g the gravitational acceleration, H the total height of the storage, T_{top} and T_{bot} are the temperatures at the top and bottom, respectively, and v_s is the average horizontal velocity of the water on the stratified surface. In the worst-case analysis, v_s corresponds to the highest velocity observed within the observation period and the thermal volumetric expansion coefficient was derived from the lowest internal temperature.

$$Ri = \frac{\beta_f g H (T_{top} - T_{bot})}{v_s^2} \tag{4}$$

3. RESULTS

In this section, the thermocline, fluid dynamics, turbulence, and stratified layer quality are discussed using the procedure in the previous section, and the quality of the CFD model is evaluated. Comparing the simulation approach with experimental data reveals its successes and limitations, which has practical implications for future stratified TES design and operation.

3.1. Thermocline Transition and RMSE

The validation study provides insights into transient thermocline dynamics and their relationship with temperature deviations. In all three scenarios, the designated sensor positions consistently exhibited exceptional and consistent temperature behavior. The simulation accurately replicates the temperature changes observed at the sensor locations in the experiments. However, it also shows localized oscillations due to internal fluid dynamics.

Distinct flow profiles are observed in the upper storage region during pure charging (Figure 8). This phenomenon is caused by the unique characteristics of the boundary conditions and the creation of a new temperature layer with a significantly lower temperature gradient of about 6 °C (refer to Figure 7), which is different from the other experiments with approximately 25 °C (refer to Figure 9 and Figure 10). The localized behavior is affected by the interaction between thermocline formation and temperature gradients, resulting in a distinct flow pattern. However, this pattern is somewhat damped in the experimental setup due to sensor inertia.

In the discharging scenario, a remarkable alignment between the simulated and experimentally measured data was attained. Nevertheless, it is worth noting that the simulation exhibits a relatively abrupt temperature transition at the measurement points during the thermal ramping of the thermocline at sensor positions 3 and 4 of Figure 9. This observation suggests that the exit regions of the experimental thermocline in reality

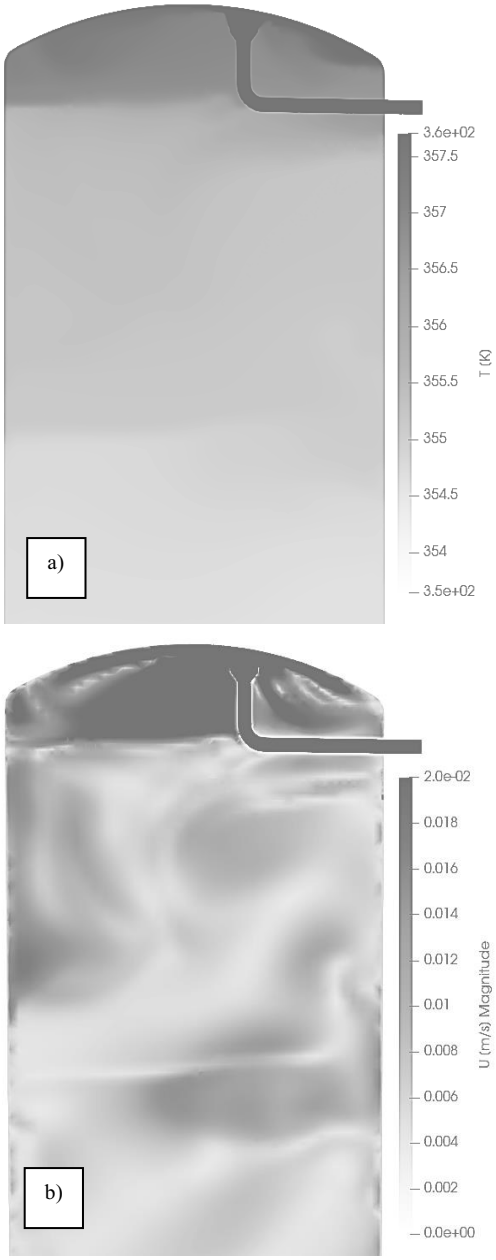

Figure 7 Origin of new thermocline in the top of the storage after 780 s of charging scenario: a) temperature profile, b) velocity profile.

exhibit a somewhat smoother transition into the respective underlying and overlying temperature zones. However, this could be rectified through a more precise predefinition of the thermocline's manifestation.

The simulation accurately replicates the thermocline dynamics at the sensor locations during simultaneous operation. The temperature profiles and thermocline dynamics exhibit a strong correlation (see Figure 10). The movement of the thermocline through the temperature sensors, along with their synchronized patterns in relation to incoming and outgoing fluids, confirms the simulation's accurate depiction of the dynamics.

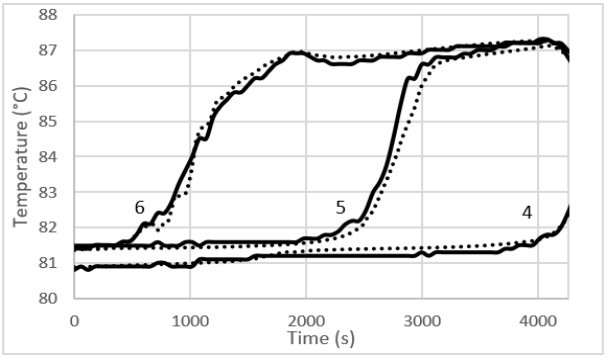

Figure 8 Experimental (solid) and simulated (dotted) temperatures of sensors 6, 5 and 4 of charging scenario.

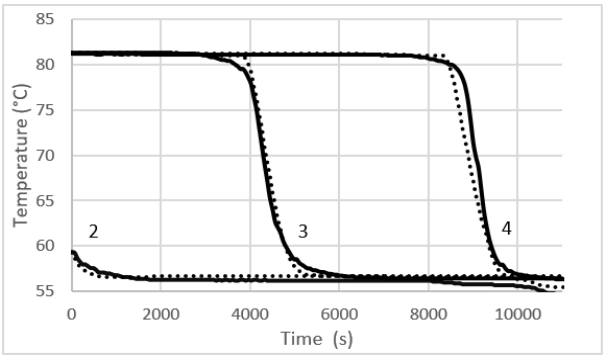

Figure 9 Experimental (solid) and simulated (dotted) temperatures of sensors 2, 3 and 4 of discharging scenario.

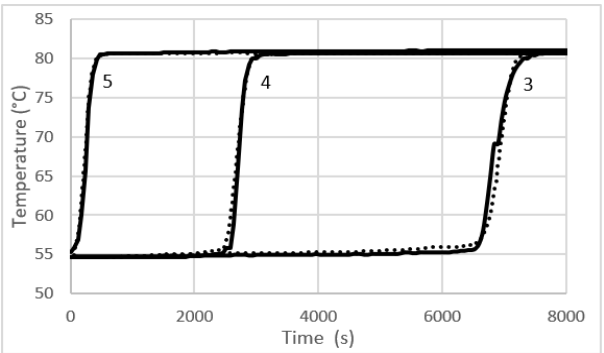

Figure 10 Experimental (solid) and simulated (dotted) temperatures of sensors 5, 4 and 3 of simultaneous scenario.

However, the limited number of measurement points and their slightly delayed response to temperature changes restrict direct inferences about internal flow profiles outside the thermocline transitions. Moreover, the precise pre-definition of the initial thickness and characteristics of the thermocline is a critical factor. The accuracy of the results is greatly affected by even a minor variation from the specified thickness, which in turn has a considerable effect on the transitions of the transient thermocline at each individual sensor.

Table 3. *RMSE* of all scenarios

Scenario	*RMSE* (°C) with sensor-positions in brackets		
Charging	0.2 (6)	0.2 (5)	0.1 (4)
Discharging	0.5 (2)	0.6 (3)	1.2 (4)
Simultaneous	0.3 (5)	0.4 (4)	1.1 (3)

Nevertheless, the simulated values closely match the experimentally determined values throughout the entire observation period of pure charging (see Table 3). In this scenario, a maximum *RMSE* of 0.2 °C is achieved over more than one hour. The inconsistent behavior of the sixth sensor is caused by the dynamic flow pattern in the upper section. Water intrusion directly impacts the thermocline dynamics, leading to pronounced local oscillations at the top sensor. The maximum *RMSE* achieved in the discharge scenario is 1.2 °C. The slight separation between thermocline transitions at sensor 4 is again due to small differences of the initial thermocline formation. Despite the challenge, the simulation accurately predicts thermocline dynamics and transitions, with discrepancies mainly occurring at thermocline boundaries. The simultaneous scenario is characterized by a maximum *RMSE* of 1.1 °C at the third temperature sensor. These small deviations can be explained by additional internal flow occurrences in the time range of thermocline transition.

In summary, although there are some localized variations, especially caused by the initial definition of the thermocline and in areas affected by fluctuations in volume flow, the simulation effectively represents the complex dynamics of thermocline behavior and temperature profiles. The *RMSE* values observed in this study align with those reported in prior research [2, 9, 11, 35], and may even partially exceed them, thereby providing evidence of a robust simulation framework.

3.2. Reynolds number

The calculation of *Re* entails using the highest velocities at the inlet of CHP and LHN, in relation to the corresponding pipe diameters. The numbers reported in Table 4 are obtained by this technique, therefore determining the flow regime.

Table 4. *Re* numbers of all scenarios for thermocline, inlet of CHP and LHN and *Ri* numbers

Scenario	$Re_{CHP}\ in$	$Re_{LHN}\ in$	Re_{th}	*Ri*
Charging	211200	---	8200	> 41
Discharging	---	27700	2300	> 974
Simultaneous	229000	62100	5800	> 452

In all scenarios, the calculated Reynolds numbers exceed the critical threshold of 2300, indicating turbulent flow in the lower and upper regions of the charging and discharging geometries. Even during unloading with significantly lower volumetric flows of the feeding devices, *Re* remains in the turbulent flow range throughout. This aligns with the use of the buoyantKEpsilon turbulence model for computation. The thermocline behavior is notably influenced in the pure charging scenario, where the velocity profile closely aligns with the developing thermocline in the upper region. This explains the thermal and turbulent patterns observed near the highest temperature sensor, as discussed earlier.

The influence on the thermocline becomes less significant in distant regions from the inlets. Inter-layer mixing is effectively prevented even in cases of internal stratification with reduced temperature gradients. This observation supports the existence of stratification patterns, even in scenarios with lower temperature differences. Figure 8a) depicts minor temperature gradients in the lower region for visual representation.

To examine this behavior in more detail, a more refined analysis of *Re* with respect to the thermocline is discussed in the following section.

3.3. Thermocline Reynolds number

The thermocline Reynolds number was calculated by analyzing the highest vertical velocities of the thermocline over the entire observation period. The storage vessel's inner diameter was used as the characteristic length for this calculation. The maximum values are presented in Table 4.

The study of thermocline stability, flow parameters, and simulation fidelity yields significant results. The pure charging scenario has a higher *Re* of 8200 due to its proximity to the inlet. As a result, noticeable changes occur in the behavior of the thermocline in this situation.

In the scenario of simultaneous charging and discharging, the thermocline remains stable despite volumetric flows of 25 m³/h from the CHP in the upper part and partly only 5 m³/h from the LHN in the lower section. Nevertheless, the thermocline *Re* of 5800 suggests a transition to turbulence.

In contrast, the discharging scenario has a low inlet velocity and a discharging rate of around 7.5 m³/h, resulting in a thermocline *Re* of 2300. This puts it close to the regime where the thermocline itself could eventually experience turbulent flow.

The study of thermocline *Re* and stability highlights the resilience of the thermocline under different conditions. However, the optimized meshing of the thermocline is able to accurately capture this behavior

and precisely map the turbulence in close vicinity to the thermocline, ensuring an accurate and reliable analysis.

3.4. Richardson Number

To enhance the precision of our analysis regarding the thermocline and its behavior, the Richardson number was calculated, following the methodology proposed by [3] and summarized within Table 4.

Remarkably, all three scenarios studied yielded values well above the already mentioned thresholds of 1 and 5, respectively, confirming the stable thermocline behavior already described in the section above. In particular, a slightly reduced *Ri* value of 41 was obtained for the charging scenario, confirming the earlier observation of a marginally stronger influence on the thermocline due to the nearby inflow. However, even in this case, the system remains in a stable region, and no significant internal flow-related disturbances are expected after the thermocline has fully developed. The even higher values of the remaining two scenarios also indicate a very high stability of the thermocline here.

4. OUTLOOK

The validation of a functional and realistic model for medium-scale stratified TES by this study has promising implications. This is an improvement in the calculation of internal flow patterns and turbulence and allows the evaluation of the influence of these on temperature stratification. It also paves the way for optimizing operational approaches and increasing system efficiency. A near-term application is planned at the Institute for Hydrogen and Energy Technology at Hof University of Applied Sciences, which has developed a complex and innovative storage concept. The facility has the potential to revolutionize the operation and management of medium-scale thermal storage systems, thereby increasing the energy efficiency of the Institute's facilities. This study has far-reaching implications beyond operational strategies. By gaining precise knowledge about the internal storage conditions, future research efforts can be focused on developing and implementing novel concepts and operational scenarios to explore the application of larger storage units in centralized energy supply systems for larger buildings such as office complexes, residential compounds, and public structures.

This institute building at the University of Applied Sciences Hof (currently under construction) will serve as a practical research facility that incorporates a flexible energy supply system capable of utilizing different renewable sources. The integrated multiple stratified mid-scale TES incorporates various charging and discharging geometries, including stratification lances, radial diffusers, and crossflow tubes, in addition to standard flanges [36]. These geometries enhance the

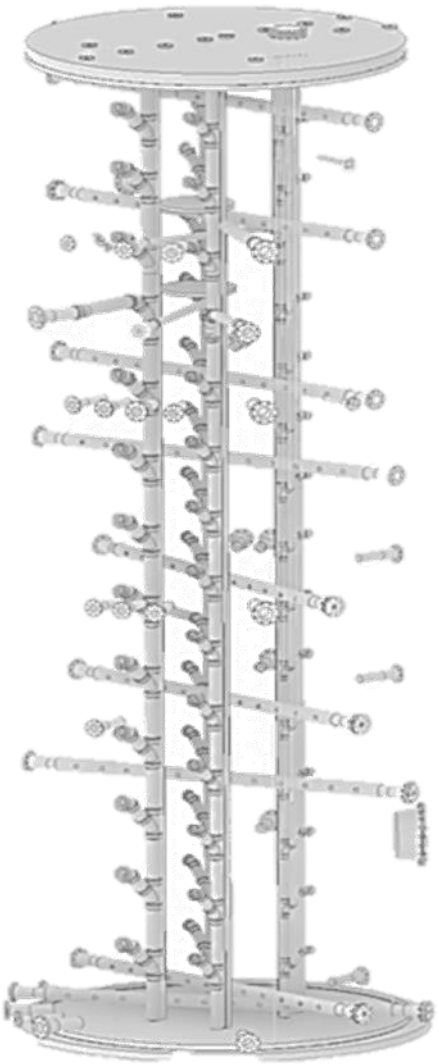

Figure 11 Insight of stratified TES at Institute for Hydrogen and Energy Technology of UAS Hof [Haase Tank GmbH]

efficiency of storing volatile heat sources and sinks. Refer to Figure 11 for visual representation. In order to enhance our model and validation methods, we additionally implement a fiber-optic temperature measurement system. This advancement offers high-resolution assessments that cover both radial and vertical dimensions, addressing the complexity of the system's operation. We will consider various operational modes and their simultaneous effects. This comprehensive approach will help us develop optimization strategies to improve system efficiency.

Integrating these refinements into the current CFD model and experimental setup will enhance our comprehension of thermal and fluid dynamics in medium-scale thermal storage systems. This will have a dual impact: advancing sustainable energy technologies and innovative building systems.

5. CONCLUSION

The simulation setup employed in this study has demonstrated the capability to realistically simulate various scenarios of larger or mid-size thermal storage systems and provide insights into thermocline behavior. It successfully replicates volatile charging and discharging flows, accompanied by fluctuating temperatures and their effects on internal stratification. Notably, thermocline stability remains robust even under relatively extreme boundary conditions and with simple charging and discharging devices examined in this investigation, with very less pronounced influence from internal vortexes or flows. The Richardson number emerges as a reliable indicator of thermocline stability, with values exceeding 5 serving as a favorable threshold as already stated by other references. The thermocline Reynolds number as an indicator of turbulent and unstable behavior of the stratification is a key figure to be emphasized. When the Reynolds number of the thermocline is below the critical Reynolds number range of 2300, laminar simulation can replace the choice of the buoyantKEpsilon turbulence model to speed up and ensure a stable simulation while maintaining high quality results.

Slight disparities in the depiction of individual thermocline transitions and temporal displacements primarily stem from imprecisely predefined thermocline thicknesses, a limitation that can be addressed through targeted pre-simulations to better predict and replicate the evolving thickness and thermocline transition. While the behavior of near-inlet thermoclines can be predicted quite effectively, special attention to detail is warranted to accurately capture and simulate potential internal vortexes that may arise.

In summary, the results and accuracy achieved through the conducted simulation studies exhibit a strong alignment with experimentally derived data. This agreement not only underlines the credibility of the CFD approach, but also provides a solid basis for further optimization and exploration of different scenarios and storage configurations.

AUTHORS' CONTRIBUTIONS

R. Fick: Conceptualization, planning and conducting experiments, data curation, methodology, visualization, writing – original draft. **R. Honke**: Methodology, supervision, writing – review and editing, funding acquisition. **D. Brüggemann**: Methodology, writing – review and editing. All authors have read and agreed to the published version of the manuscript.

ACKNOWLEDGMENTS

The authors gratefully acknowledge the support of the Bavarian State Ministry of Education, Science and the Arts within the framework Graduiertenkolleg Energieautarke Gebäude of the TechnologieAllianzOberfranken (TAO). In addition, the authors gratefully acknowledge financial support from the German Federal Ministry for Economic Affairs and Climate Action (BMWK) under the 7th Energy Research Program with the funded project OUR-E (grant number 03EN6023A). Special thanks also go to Mr. Reinhold Behr from the local heating network Großbardorf for his active support, collection, and provision of the measurement data. In addition, the authors would like to express special thanks to Mr. Jan Diriken and Mr. Johann van Bael of VITO - Vlaamse Instelling voor Technologisch Onderzoek for providing experimental data for initial simulation setup and tuning.

REFERENCES

[1] S. M. Hosseinnia, H. Akbari and M. Sorin, Numerical analysis of thermocline evolution during charging phase in a stratified thermal energy storage tank, Journal of Energy Storage, Volume 40, 2021, p. 102682. DOI: 10.1016/j.est.2021.102682.

[2] B. Baeten, T. Confrey, S. Pecceu, F. Rogiers and L. Helsen, A validated model for mixing and buoyancy in stratified hot water storage tanks for use in building energy simulations, Applied Energy, Volume 172, 2016, pp. 217-229. DOI:10.1016/j.apenergy.2016.03.118.

[3] T. Chekifi and M. Boukraa, CFD applications for sensible heat storage: A comprehensive review of numerical studies, Journal of Energy Storage, Volume 68, 2023, p. 107893. DOI: 10.1016/j.est.2023.107893.

[4] T. Bouhal, S. Fertahi, Y. Agrouaz, T. E. Rhafiki, T. Kousksou and A. Jamil, Numerical modeling and optimization of thermal stratification in solar hot water storage tanks for domestic applications: CFD study, Solar Energy, Volume 157, 2017, pp. 441-455. DOI: https://doi.org/10.1016/j.solener.2017.08.061.

[5] Y. Deng, D. Sun, M. Niu, B. Yu and R. Bian, Performance assessment of a novel diffuser for stratified thermal energy storage tanks – The nonequal-diameter radial diffuser, Journal of Energy Storage, Volume 35, 2021, p. 102276. DOI: 10.1016/j.est.2021.102276.

[6] Y. Xiang, M. Gao, S. Furbo, D. Wang, Z. Tian and J. Fan, Heat transfer of a large-scale water pit heat storage under transient operations, Journal of

Energy Storage, Volume 55, 2022, p. 105455. DOI: 10.1016/j.est.2022.105455.

[7] L. Kocijel, V. Mrzljak and V. Glažar, Conversion of A medium heavy heating oil tank into A heat storage tank, Heat Mass Transfer, Volume 56, 2020, pp. 871-890. DOI: 10.1007/s00231-019-02751-6.

[8] H. K. B. Sangjoeei, CFD Simulation of Stratified Thermal Energy Storage Tank Ecovat, Ecovat Team, 2021. https://www.ecovat.eu/wp-content/uploads/2021/06/Ecovat-CFD-Simulation-V1.01.pdf, retrieved on: 08.03.2023.

[9] A. Soares, J. Camargo, J. Al-Koussa, J. Diriken, J. van Bael and J. Lago, Efficient temperature estimation for thermally stratified storage tanks with buoyancy and mixing effects, Journal of Energy Storage, Volume 50, 2022, p. 104488. DOI: 10.1016/j.est.2022.104488.

[10] S. Jian, H. Jing, F. Lin and Z. Shigang, Experimental study of a large temperature difference thermal energy storage tank for centralized heating systems, Thermal Science, Volume 22, Issue 1 Part B, 2018, p. 613–621. DOI: 10.2298/TSCI160720173S.

[11] J. Rendall, F. Karg Bulnes, K. Gluesenkamp, A. Abu-Heiba, W. Worek and K. Nawaz, A Flow Rate Dependent 1D Model for Thermally Stratified Hot-Water Energy Storage, Energies, Volume 14, No. 9, 2021, p. 2611. DOI: 10.3390/en14092611.

[12] S. e.-D. Fertahi, A. Jamil and A. Benbassou, Review on Solar Thermal Stratified Storage Tanks (STSST): Insight on stratification studies and efficiency indicators, Solar Energy, Volume 176, 2018, pp. 126-145. DOI: https://doi.org/10.1016/j.solener.2018.10.028.

[13] F. E.-A. Mohamed and A.-G. Abdulmajeed, Experiments and numerical simulation for a thermal vertical jet into a rectangular water tank, Results in Physics, Volume 10, 2018, pp. 680-692. DOI: 10.1016/j.rinp.2018.07.016.

[14] S. Göppert, R. Lohse, T. Urbaneck, U. Schirmer, B. Platzer and P. Steinert, New computation method for stratification pipes of solar storage tanks, Solar Energy, Volume 83, No. 9, 2009, p. 1578–1587. DOI: 10.1016/j.solener.2009.05.007.

[15] W. Lou, B. Xie, J. Aubril, Y. Fan, L. Luo and A. Arrivé, Optimized flow distributor for stabilized thermal stratification in a single-medium thermocline storage tank: A numerical and experimental study, Energy, Volume 263, Part A, 2023, p. 125709. DOI: https://doi.org/10.1016/j.energy.2022.125709.

[16] W. Lou, Y. Fan and L. Luo, Single-tank thermal energy storage systems for concentrated solar power: Flow distribution optimization for thermocline evolution management, Journal of Energy Storage, Volume 32, 2020, p. 101749. DOI: https://doi.org/10.1016/j.est.2020.101749.

[17] X.-W. Xu, A. Haghiria, R. D. Sandberg, T. Oda and K. Tanimoto, Large Eddy Simulation and Turbulence Model Assessment for Buoyant Flow in a Thermal Energy Storage Tank, available at SSRN: https://ssrn.com/abstract=4410549, retrieved on 30.08.2023. DOI: http://dx.doi.org/10.2139/ssrn.4410549.

[18] A. Li, F. Cao, W. Zhang, B. Shi and H. Li, Effects of different thermal storage tank structures on temperature stratification and thermal efficiency during charging, Solar Energy, Volume 173, 2018, pp. 882-892. DOI: 10.1016/j.solener.2018.08.025.

[19] A. Karim, A. Burnett and S. Fawzia, Investigation of Stratified Thermal Storage Tank Performance for Heating and Cooling Applications, Energies, Volume 11, 2018, p. 1049. DOI: 10.3390/en11051049.

[20] S. F. Corzo, D. E. Ramajo and N. M. Nigro, High-Rayleigh heat transfer flow, Thermal stratification analysis and assessment of Boussinesq approach, International Journal of Numerical Methods, Volume 27, No. 9, 2017, pp. 1928–1954. DOI: 10.1108/HFF-05-2016-0176.

[21] R. Kumar and A. Dewan, URANS computations with buoyancy corrected turbulence models for turbulent thermal plume, International Journal of Heat and Mass Transfer, Volume 72, 2014, p. 680–689. DOI: 10.1016/j.ijheatmasstransfer.2014.01.066.

[22] R. John, Validierung eines Rechenmodells für Großspeicher zur Auslegung solarer Heizsysteme, Philipps-Universität Marburg, Dissertation, 2002.

[23] J. Lago, F. d. Ridder, W. Mazairac and B. d. Schutter, A 1-dimensional continuous and smooth model for thermally stratified storage tanks including mixing and buoyancy, Applied Energy, Volume 248, 2019, p. 640–655. DOI: 10.1016/j.apenergy.2019.04.139.

[24] M.-S. Shin, H.-S. Kim, D.-S. Jang, S.-N. Lee, Y.-S. Lee and H.-G. Yoon, Numerical and experimental study on the design of a stratified thermal storage system, Applied Thermal Engineering, Volume 24, Issue 1, 2004, pp. 17-27. DOI: 10.1016/S1359-4311(03)00242-4.

[25] R. Huhn, Beitrag zur thermodynamischen Analyse und Bewertung von Wasserwärmespeichern in Energieumwandlungsketten, TU Dresden, Dissertation, 2006.

[26] H. Khurana, R. Majumdar and S. Saha, Thermal Stratification Characteristics during Simultaneous Charging and Discharging for Different Storage Tank Geometries with Immersed Discharging Coil, Applied Thermal Engineering, Volume 225, 2023, p. 120235. DOI: 10.1016/j.applthermaleng.2023.120235.

[27] C. Liu, W. Zhao, J. Wang and D. Wan, Improving the numerical robustness of buoyancy modified k-ω SST turbulence model, Marine VIII, proceedings of the VIII International Conference on Computational Methods in Marine Engineering, 2019, pp. 514-524. ISBN: 978-84-949194-3-5.

[28] Y. P. Chandra and T. Matuska, Numerical prediction of the stratification performance in domestic hot water storage tanks, Renewable Energy, Volume 154, 2020, pp. 1165-1179. DOI: https://doi.org/10.1016/j.renene.2020.03.090.

[29] A. Herwig, L. Umbreit and K. Rühling, Temperaturfeldmessung in Großwärmespeichern von KWK-basierten Fernwärmesystemen als Werkzeug zur Effizienzsteigerung, final report, TU Dresden, 2019.

[30] F. Findeisen, T. Urbaneck and B. Platzer, Radial Diffusers in Stratified Hot Water Stores: Geometry Optimization with CFD, proceedings of ISES Solar World Congress 2017, 2017, pp. 726-734. DOI: 10.18086/swc.2017.13.04.

[31] T. Yang, W. Liu, G. J. Kramer and Q. Sun, Seasonal thermal energy storage: A techno-economic literature review, Renewable and Sustainable Energy Reviews, Volume 139, 2021, p. 110732. DOI: 10.1016/j.rser.2021.110732.

[32] C. Greenshields, OpenFOAM v8 User Guide, The OpenFOAM Foundation, 2020. https://doc.cfd.direct/openfoam/user-guide-v8, retrieved on 30.08.2023.

[33] T. Cebeci and J. Cousteix, Conservation Equations for Mass, Momentum and Energy. Modeling and Computation of Boundary-Layer Flows, Springer, Berlin, Heidelberg, 2005, pp. 17-25. DOI: 10.1007/3-540-27624-6_10.

[34] OpenCFD Ltd., OpenFOAM: API Guide v2112, buoyantKEpsilon, 2023. https://www.openfoam.com/documentation/guides/latest/api/classFoam_1_1RASModels_1_1buoyantKEpsilon.html, retrieved on 30.08.2023.

[35] J. Rendall, F. K. Bulnes, K. Gluesenkamp, A. Abu-Heiba, W. Worek and K. Nawaz, Comparison of plug flow and multi-node stratified tank modeling approaches regarding computational efficiency and accuracy, International Mechanical Engineering Congress and Exposition (IMECE2020) - Portland, Oregon, United States of America, 2020. OSTI: https://www.osti.gov/servlets/purl/1756251.

[36] R. Fick, O. Stark, R. Honke and T. Plessing, Innovatives Versorgungskonzept zur multiplen Nutzung erneuerbarer Energiequellen des Instituts für Wasser- und Energiemanagement, proceedings of RET.Con 2022, 2022, pp. 82-93. ISBN: 978-3-940820-19-8.